WILEY | Hindawi

Research Article

High-Strength Hollow Glass Microsphere/Epoxy Resin Composite Insulation Materials for Deep *In-Situ* Condition Preserved Coring

Jianping Yang,[1,2] **Ling Chen** ⓘ,[3] **Zhiqiang He** ⓘ,[4] **Cong Li,**[4] **Bo Yu,**[3] **Zijie Wei,**[4] **Zhiyu Zhao** ⓘ,[5] **and Zongxin Hao**[6]

[1]*Institute of Deep Earth Sciences and Green Energy, College of Civil and Transportation Engineering, Shenzhen University, Shenzhen 518060, China*
[2]*College of Polymer Science and Engineering, Sichuan University, Chengdu 610065, China*
[3]*School of Mechanical Engineering, Sichuan University, Chengdu 610065, China*
[4]*College of Water Resource & Hydropower, Sichuan University, Chengdu 610065, China*
[5]*Institute of New Energy and Low-Carbon Technology, Sichuan University, Chengdu, 610065 Sichuan, China*
[6]*China Construction First Group the Fifth Construction Co., Ltd, Beijing 100024, China*

Correspondence should be addressed to Ling Chen; chenlingscu@scu.edu.cn

To establish *in-situ* fluidized coal mining technology and a theory of mining mechanics for deep coal resources, it is crucial to obtain a "fidelity rock core" that maintains deep *in-situ* conditions to understand the physical mechanics of deep rock. Doing so requires the development of *in-situ* condition-preserved coring (ICP-coring) technology. In this work, hollow glass microsphere/epoxy resin (HGM/EP) composite insulation materials with high strengths were prepared. An epoxy resin matrix with high strength and high-temperature resistance was selected from among epoxy resins cured by different curing agents. Then, a series of composite insulation materials with different HGM volume fractions were prepared. The mechanical strengths of the composites decreased with increasing HGM volume fraction. Then, thermal insulation materials suitable for different ICP-coring depths were selected. Changes in the thermal conductivities and mechanical strengths of the composites were characterized after they were subjected to high water pressure (45 MPa). Verification of the applicability of the thermal insulation material under high water pressure (45 MPa) conditions demonstrated that it met the working requirements for the ICP-coring device.

1. Introduction

China's total coal consumption remains high, and traditional coal mining and utilization produce large amounts of carbon dioxide emissions and environmental pollution [1]. According to China's energy development strategy, coal will remain the basic energy source for a long time [2]. Shallow coal resources are becoming exhausted, and the depth of underground mining is gradually increasing and has currently reached around 1500 m [3, 4]. Nearly 70% of China's coal resources are distributed below 2000 m. Therefore, mining deep coal resources is imperative [5].

Considerable experience in mining shallow coal resources has accumulated. However, deep coal resources are very different from shallow coal resources [6, 7], and the deep environment is characterized by "high temperature, high stress, and high osmotic pressure" [8–10]. Temperature has a significant impact on the physical and mechanical properties and permeability of rock [11–14]. Current basic research on the development of deep coal resources is highly insufficient [15]. Traditional research on rock characteristics is based on the establishment of an "ordinary core" that has lost its *in-situ* temperature and osmotic pressure [16]. When faced with the limitations of the deep formation

environment, traditional mining and mechanics theories are unable to solve the technical problems of deep coal mining [17, 18]. There are severe challenges to the green, safe, and efficient production of deep coal [19]. *In-situ* fluidized coal mining is expected to break through the depth limit of coal resource mining; address the low production efficiency, poor safety, and poor resource exploitation rate faced in the mining industry; and reform the mining of deep coal resources [20, 21]. To establish *in-situ* fluidized coal mining technology and a dynamics theory for deep mining of coal resources, it is crucial to explore the physical mechanics of rock at different depths [22]. A "fidelity rock core" that maintains deep *in-situ* conditions is essential and can be obtained through *in-situ* condition-preserved coring (ICP-coring) technology [23, 24].

Every 100 m below the surface, the rock temperature increases by approximately 3°C. Therefore, deep rocks and shallow rocks have very different temperatures [25]. For example, at a depth of 5000 m, the rock core temperature can reach approximately 150°C. Maintaining the *in-situ* temperature of a deep rock core requires the development of a set of *in-situ* temperature-preserved coring (ITP-coring) devices. An effective method for ITP-coring is to add an insulation layer to the coring device [26]. Sun et al. [27] used frozen alcohol as an insulation layer to maintain the low temperatures of natural gas hydrate (NGH) cores. The pressure-temperature core sampler (PTCS) uses an adiabatic inner tube as the insulation layer and maintains the low temperature of NGH cores by using the Peltier effect [28]. However, these thermal insulation coring devices are intended to maintain the low temperatures of NGH cores [29, 30], whereas the goal in obtaining deep *in-situ* rock cores is to maintain high temperatures. Both the First Oceanographic Institute of China and PTPS add a vacuum layer to the coring device as an insulation layer [31, 32], but this approach reduces the impact strength of the coring device while increasing its volume and cost.

Zhu et al. proposed using polyurethane foam as the thermal insulation material for coring devices [33]. However, polyurethane foam has poor water resistance and loses its thermal insulation capacity in deep high-pressure water environments. Polyurethane has low compressive strength and requires additional reinforcement layer. Therefore, polyurethane foam is not the best choice for insulating a deep coring device.

To realize temperature-preserved coring of a deep ITP-coring system within a small volume, thermal insulation materials with high compressive strength and high thermal stability are needed [34]. A high-strength insulation material can be used as the insulation layer of the coring device without an added reinforcement layer, which would reduce the size of the coring device compared with a device with a vacuum or polyurethane insulation layer. Epoxy resin (EP) is a thermosetting polymeric material with excellent mechanical properties and low thermal conductivity [35]. Hollow glass microspheres (HGMs) are microspheres with hollow structure and low thermal conductivity [36]. Based on the properties of EP and HGMs, high-compressive-strength insulation materials suitable for ITP-coring devices can be

prepared. Here, the EP matrix material with the highest compressive strength was selected from among EPs with different curing agents. High-strength HGM/EP composite insulation materials suitable for different coring depths were obtained. The influence of the HGM volume fraction on the properties of the composite materials was investigated.

2. Experimental

2.1. Materials

2.1.1. Epoxy Resin. EP prepolymer is an epoxy oligomer that is liquid at room temperature. It can be cured under certain conditions and transformed into a rigid thermosetting resin with a three-dimensional network structure. EP exhibits minimal shrinkage during curing from a liquid to a solid, and the cured material has high mechanical strength, high thermal stability, and strong corrosion resistance. Therefore, it is suitable for preparing a matrix of high-strength insulation material [37].

The epoxy prepolymer used in this study was bisphenol A diglycidyl ether, resin E51, which is a transparent liquid. The viscosity was approximately 2500 mPa·s (40°C), the epoxy value was 0.48–0.54 (mol/100 g), the hydroxyl value was 0.23–0.28 (mol/100 g), and the polymerization degree was 0.2–0.6.

2.1.2. Hollow Glass Microspheres. HGMs have smooth surfaces and simple structures and are generally regular and spherical. The key feature is a cavity structure with a very large volume ratio [38], which contains air, inert gas, and so on. Due to their unique structure, HGMs exhibit many excellent properties, such as low density, low thermal conductivity, good sound insulation performance, and high electrical insulation performance [39].
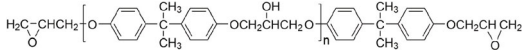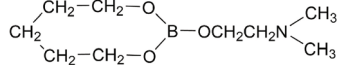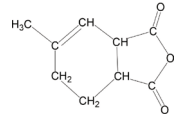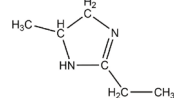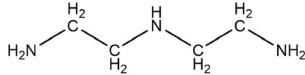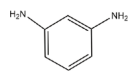
The HGMs used in this experiment were K1 HGMs provided by 3M, which had a compressive strength of 1.72 MPa, thermal conductivity of 0.047 W/m·K, and density of 0.125 g/cm^3.

2.1.3. Other Materials. The sources and structural formulas for other chemical materials used in the study are shown in Table 1.

2.2. EP Selection. EP E51 reacts with the curing agent to produce a high-strength EP matrix. CICG, 594, AEEA, 2E4MI, and mPDA were used as curing agents according to the compressive strength desired for the cured EP and the difficulty of composite material preparation. Curing processes for different curing agents were explored, and a series of EP matrix samples with different curing agents were prepared to identify an EP matrix with high mechanical strength and high-temperature resistance. The compressive strengths and thermal decomposition temperatures of the different prepared EPs are shown in Figures 1 and 2.

Figure 1 shows that the EP matrix cured with mPDA had the highest strength, which reached approximately 194 MPa. This high strength is attributable to the rigid and stable benzene ring structure of mPDA, which reduced the extent of kneading for EP chain segments and enhanced their rigidity.

TABLE 1: Information on experimental materials.

| Name	Purity	Manufacturer	Molecular formula
Common industrial curing agent (CICA)	Industrial grade	Jinghong Polymer Materials Co., Ltd.	—
EP E51	Industrial grade	Nantong Xingchen Synthetic Co., Ltd.	
594 boramine curing agent (594)	Industrial grade	China National Bluestar (Group) Co., Ltd.	
Methyltetrahydrophthalic anhydride	Industrial grade	China National Bluestar (Group) Co., Ltd.	
Diethyltetramethylimidazole (2E4MI)	Analytical reagent	Shanghai Macklin Biochemical Co., Ltd.	
Hydroxyethyl aminoethylethanolamine (AEEA)	Analytical reagent	Shanghai Macklin Biochemical Co., Ltd.	
m-Phenylenediamine (mPDA)	Analytical reagent	Chengdu Kelong Chemicals Co., Ltd.	
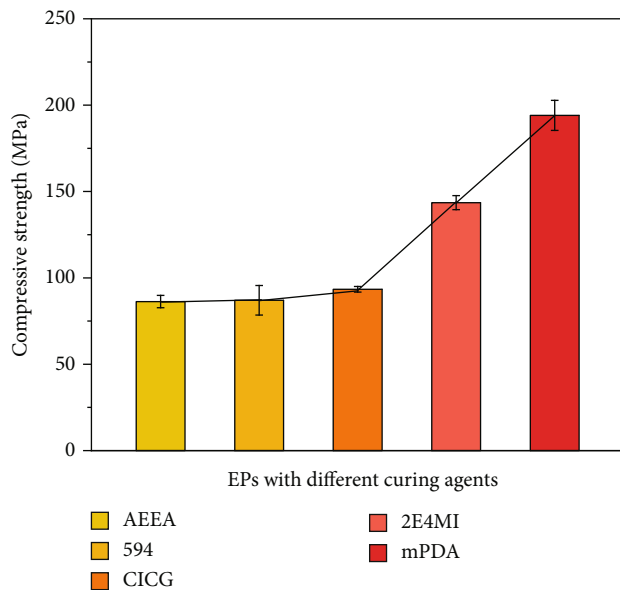
FIGURE 1: Compressive strengths of EP matrixes prepared with different curing agents. The compressive strengths of EP cured by AEEA, 594, CICA, 2E4MI, and mPDA were 82.28 MPa, 87.01 MPa, 93.4 MPa, 143.55 MPa, and 194.09 MPa, respectively.

Figures 2 and 3 show that the initial thermal decomposition temperature of E51 EP was 231.0°C before curing. After curing with mPDA, the initial decomposition temperature of E51 EP increased to 352.2°C. Although mPDA EP did not have the highest thermal stability, it fully met the application requirements for deep ITP-coring devices. Therefore, mPDA was finally selected as the curing agent for the EP matrix.

2.3. Preparation of HGM/EP Composite Insulation Materials. Thermal insulation materials composed of HGMs and EP exhibit high compressive strength and low thermal conductivity. The composite materials are fluid before curing, which is useful for manufacturing. Based on previous experimental results [34], K1 HGMs were selected for compounding with EP, and composite insulation materials with HGM volume fractions of approximately 10%, 20%, 30%, 40%, 50%, and 60% were successfully prepared. These composites exhibited different compressive strengths and thermal insulation performances and can be used in ITP-coring devices operating at different depths.

The detailed preparation process of the composite materials was as follows:

(1) According to the density of each component and the ratio of the curing agent to E51, the required mass of each component was determined, and the raw materials were weighed according to the calculated mass

(2) E51 and mPDA were heated in an oven at 80°C for 20 min. K1 HGMs and E51 were mixed and stirred with a mechanical mixer at a stirring speed of 60 rpm for 40 min. Then, mPDA was added and stirred for 20 min

(3) The polytetrafluoroethylene molds that were filled with the composite prepolymer were placed in an oven at 50°C for 1 h, 80°C for 6 h, and 180°C for 3.5 h. Finally, the prepared sample was demolded

2.4. High-Pressure Water-Loading Experiments. To verify the resistance of the composite insulation materials to high-pressure water, the samples were placed in a high-pressure
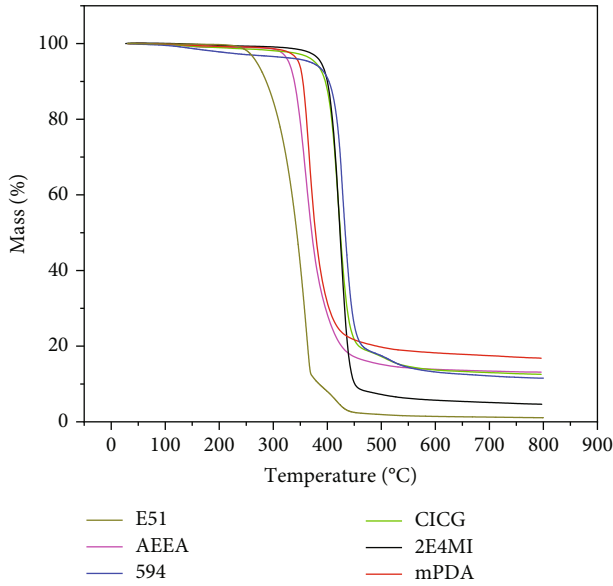
FIGURE 2: Thermogravimetric (TG) curves of the EP matrixes. The initial thermal decomposition temperatures of E51 EP, AEEA EP, 594 EP, CICG EP, 2E4MI EP, and mPDA EP were 231.0°C, 336.2°C, 368.4°C, 400.5°C, 403.7°C, and 352.2°C, respectively. The ending thermal decomposition temperatures of E51 EP, AEEA EP, 594 EP, CICG EP, 2E4MI EP, and mPDA EP were 459.95°C, 394.5°C, 490.3°C, 441.3°C, 440.5°C, and 392.9°C, respectively.
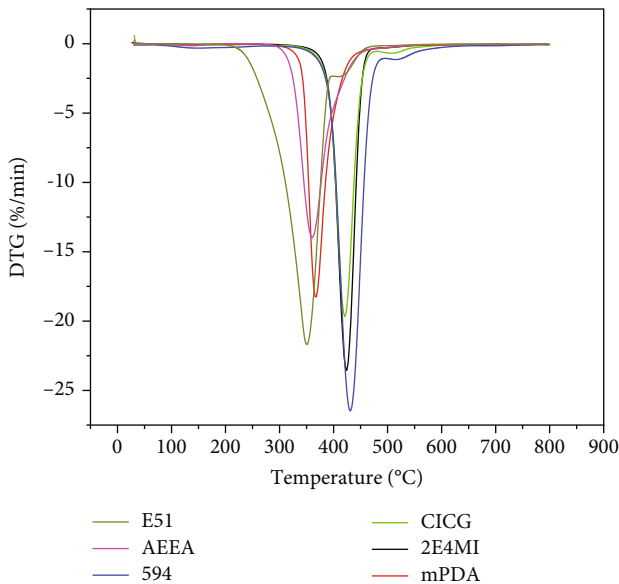

FIGURE 3: Derivative thermogravimetry (DTG) curves of the EP matrixes. The peak thermal decomposition temperatures of E51 EP, AEEA EP, 594 EP, CICG EP, 2E4MI EP, and mPDA EP were 342.9°C, 360.4°C, 430.16°C, 420.7°C, 424.0°C, and 367.1°C, respectively.

water environment. A 45 MPa high-pressure water environment was provided by equipment constructed in our laboratory, and the pressure-loading speed was controlled at approximately 10 MPa/min. After reaching the preset pressure, the pressure

was stabilized for 2 h. The properties of the composite materials were characterized after high-pressure water-loading experiments.

2.5. Characterization Methods

2.5.1. Density. Using a model MDY350 true density-measuring instrument (Zhengzhou Huazhi Technology Co., Ltd., China), the gas displacement method was employed to test the densities of the composite materials.

2.5.2. Water Absorption. The composite materials were placed in water at atmospheric and high pressure (45 MPa) for 2 h each.

2.5.3. Scanning Electron Microscopy (SEM). SEM images of the composite material cross-sections were obtained by Apreo S HiVoc (Thermo Fisher Scientific Co., Ltd., the United States of America) and SU8220 (Hitachi Co., Ltd., Japan) with high voltages of 8 kV and 10 kV, respectively.

2.5.4. Mechanical Properties. The compressive strengths of the composite materials were tested with a model 5967 instrument (Instron Co., Ltd., the United Kingdom). The compression tests were carried out according to GBT1041-1992.

2.5.5. Thermal Insulation. The thermal conductivities of the composite materials were tested with a hot disk device TPS7 (Hot Disk Co., Ltd., Sweden) with a test probe of 5465.

2.5.6. Thermal Stability. TG and TGA were measured with a TA Q50 system (TA Instruments Co., Ltd., the United States of America) with a heating rate of 10°C/s from 50 to 800°C under a nitrogen flow rate of 50 mL/min.

3. Results and Discussion

3.1. Morphology

3.1.1. HGMs. Figure 4 shows that the K1 HGMs had smooth surfaces and completely spherical structures. Most of the particle sizes were less than 65μm. Small HGMs were observed in the gaps between large HGMs. Therefore, the different particle sizes of the HGMs were conducive to the use of one EP while filling more volume with the HGMs.

3.1.2. HGM/EP Composite Insulation Materials. As shown in Figure 5, with low levels of HGM filling, the HGMs appeared to be stratified in the EP matrix. This is because the EP was a liquid before curing, and the K1 HGMs floated upward during curing because their density was lower than that of the liquid. Therefore, the composite materials with lower volume fractions of HGMs had hierarchical structures. In the temperature-preserved part of the ITP-coring device, due to the lower distributions of HGMs, the higher mechanical strengths of the composite materials, this strength-enhanced layer directly contacted the outside of the ITP-coring device. The insulating layer contained a more concentrated distribution of HGMs close to the sides of the ITP-coring device.
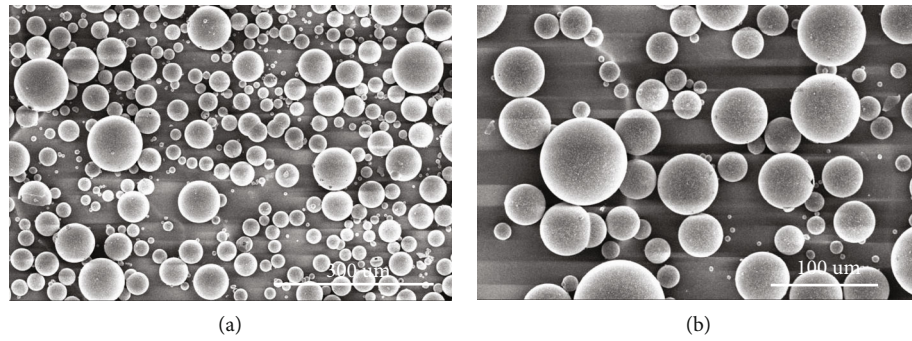
(a)

(b)

FIGURE 4: SEM images of K1 HGMs.

(a)

(b)

(c)

(d)

(e)

(f)
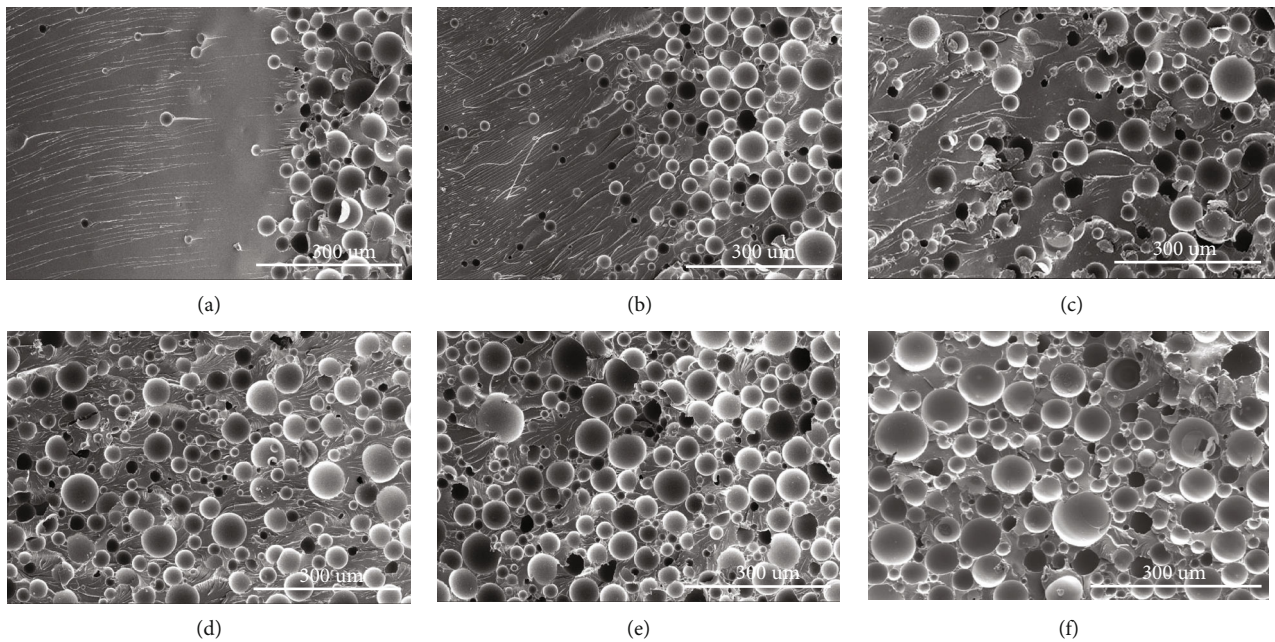
FIGURE 5: HGM/EP composite insulation materials with different HGM volume fractions: (a) 10%, (b) 20%, (c) 30%, (d) 40%, (e) 50%, and (f) 60%.
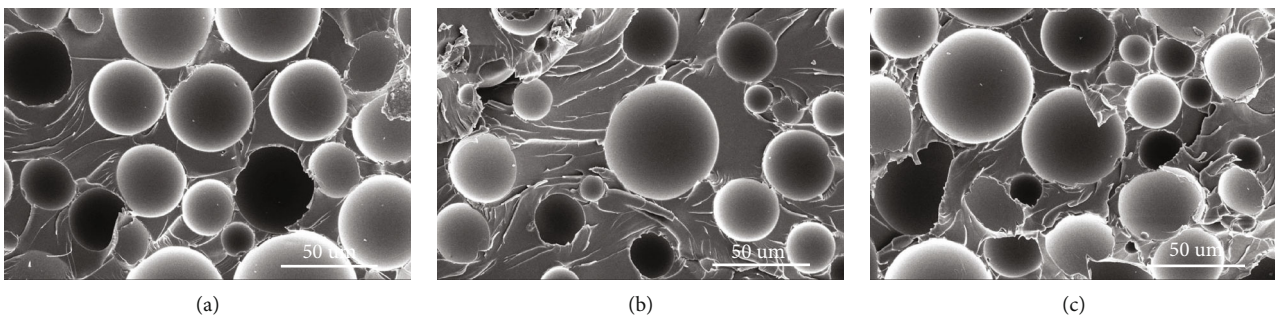

(a)

(b)

(c)

FIGURE 6: Compatibility of HGMs with the EP matrix with volume fractions of (a) 20%, (b) 40%, and (c) 50%.

When the volume fraction of the HGMs was increased to 40%, the distribution became more uniform, and the stratification almost disappeared. Figure 5 shows that when the HGM volume fraction was increased gradually, the number of broken HGMs also increased. HGMs were destroyed dur-

ing the mixing process. The extent of mutual extrusion between HGMs increased when more HGMs were added, which is more likely to lead to stress concentration and fragmentation of HGMs. When the volume fraction of the HGMs was increased to 60%, the HGMs were extruded in
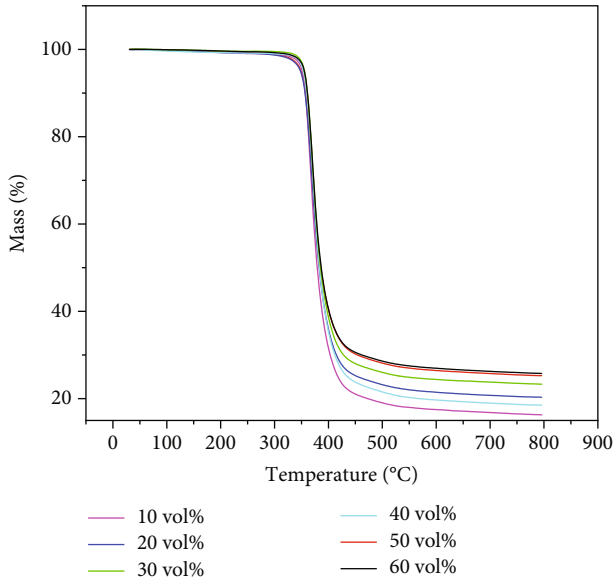
FIGURE 7: TG curves of the HGM/EP composite insulation materials. The initial thermal decomposition temperatures of the HGM/EP composite insulation materials with HGM volume fractions of 10 vol%, 20 vol%, 30 vol%, 40 vol%, 50 vol%, and 60 vol% were 354.3°C, 351.7°C, 356.5°C, 356.5°C, 353.9°C, and 356.0°C, respectively. The ending thermal decomposition temperatures were 392.1°C, 396.3°C, 395.5°C, 394.4°C, 394.5°C, and 394.8°C, respectively.
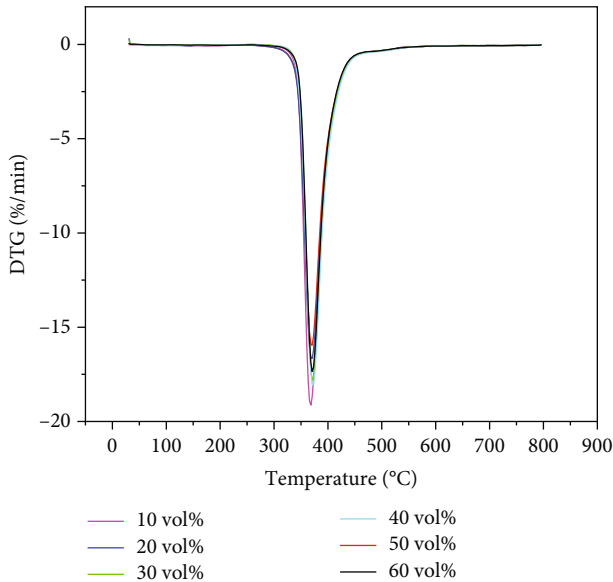

FIGURE 8: DTG curves of the HGM/EP composite insulation materials. The peak thermal decomposition temperatures for the HGM/EP composite insulation materials with HGM volume fractions of 10 vol%, 20 vol%, 30 vol%, 40 vol%, 50 vol%, and 60 vol% were 368.0°C, 369.8°C, 371.9°C, 371.4°C, 369.7°C, and 371.1°C, respectively.

the EP matrix, and more HGMs were broken. It is likely that further increasing the HGM volume fraction will result in greater HGM destruction due to interference contact [40].
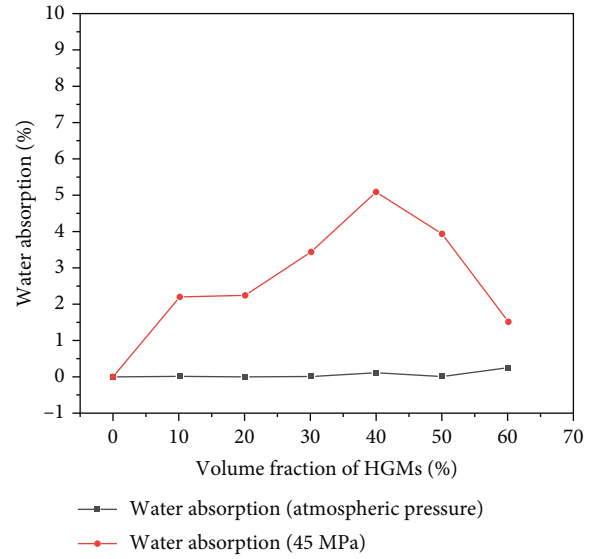

FIGURE 9: Water absorption curves of the HGM/EP composite insulation materials.

Figure 6 shows that there was a natural connection between the HGMs and the EP matrix, which showed good compatibility and no obvious gaps. This was conducive to improving the overall strengths of the composites [41]. Figure 6 shows that HGMs with smaller particle sizes were distributed in the gaps generated by HGMs with larger particle sizes, which confirmed that different HGM particle sizes were conducive to filling with more HGMs.

3.2. Thermal Stability. The temperature of the deep *in-situ* environment is very high. When the coring depth reaches approximately 5000 m, the ground temperature can reach approximately 150-200°C. Common thermal insulation materials decompose at these temperatures, the structure of the material is destroyed, and thermal insulation and mechanical strength are lost. Therefore, it is necessary to determine the thermal stabilities of the composite insulation materials. Figure 7 shows that the residual masses of the composite materials increased with increasing HGM volume fraction. Furthermore, according to Figure 8, the addition of HGMs did not reduce the thermal stability of the EP, and the temperatures of the initial thermal decomposition of the composite materials were stable and above 350°C, fully meeting the requirements for ITP-coring. Figures 7 and 8 show that the introduction of HGMs slightly improved the initial thermal decomposition temperatures of the composite insulation materials and enhanced their thermal stabilities. The addition of HGMs reduced the thermal conductivity of the material. Therefore, the external temperature must be increased to achieve the same thermal effect for the composite materials.

3.3. Water Resistance. Deep *in-situ* core-taking occurs under high-pressure water conditions. Since the thermal conductivity of water is higher than those of thermal insulation materials, water absorption leads to increases in the thermal conductivities of the materials and reduced thermal
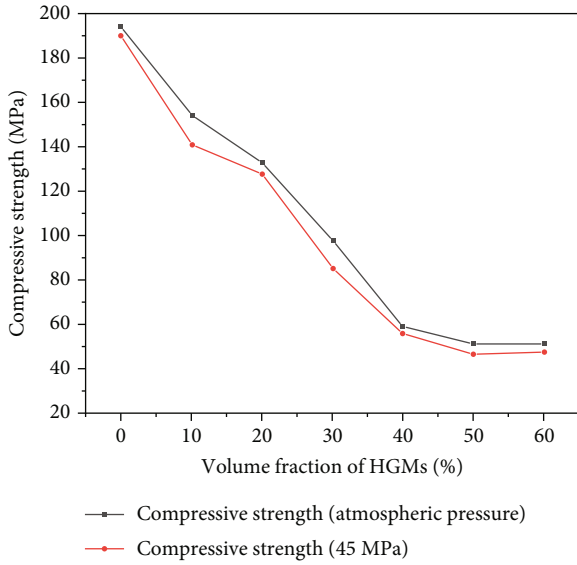
FIGURE 10: Compressive strength curves of the HGM/EP composite insulation materials.
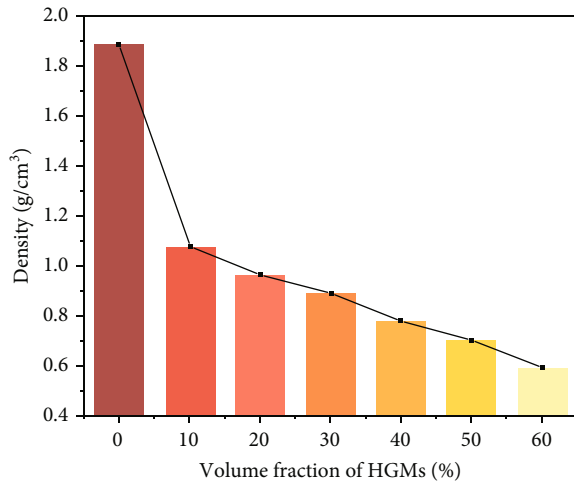

FIGURE 11: Densities of the HGM/EP composite insulation materials with the indicated HGM volume fractions.

insulation performance. After water absorption, the original structure of the material is destroyed, which affects its mechanical strength. Therefore, it is necessary to quantify the water absorption of the insulation materials. As shown in Figure 9, the water absorption rates for the composite materials were almost 0% under atmospheric pressure, which indicated that the overall structures of the materials were very dense and without loose pores. After immersion in water with a pressure of 45 MPa for 2 h, the composite materials absorbed water to varying degrees, but the highest water absorption percentage did not exceed 5.5%. The surface of the insulation material was ground and polished during sample preparation, which led to fragmentation of HGMs on the surface of the composite material and the formation of pores into which high-pressure water could be
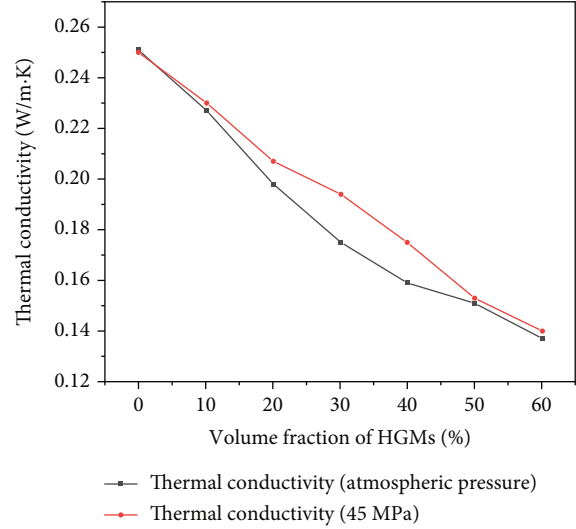

FIGURE 12: Thermal conductivity curves of the HGM/EP composite insulation materials.

injected. However, in the actual coring process, the material will absorb less water. Therefore, in terms of water resistance, the insulation material can be used with a water pressure of 45 MPa.

3.4. Mechanical Properties. Deep *in-situ* core-taking involves high ground pressures, and thermal insulation materials with low compressive strength will be squeezed and broken, reducing their thermal insulation capability. Therefore, the compressive strength of the thermal insulation material is a key performance factor. High-strength EP provides thermal insulation materials with high overall compressive strengths [42, 43]. The strengths of the HGMs used were much lower than that of the EP matrix. Figure 10 shows that the strengths of the composite materials decreased gradually with increasing HGM volume fraction. When the HGM filling level reached 50%, the compressive strength of the composite material was stable at approximately 50 MPa. However, when the HGM volume fraction exceeded 60%, the composite materials had a relatively high viscosity before curing. Further increases in the volume fraction of HGMs would lead to uneven dispersion of the HGMs and difficulties in molding the material. Consequently, the maximum HGM volume fraction used for the composite insulation materials was 60%.

After immersion in water at a pressure of 45 MPa for 2 h, the compressive strengths of the composite materials decreased slightly, and the maximum reduction ratio did not exceed 13%. When the filling amount of HGMs was 60 vol%, the compressive strength reached 47.5 MPa after immersion in water at a pressure of 45 MPa for 2 h.

Composite materials with different HGM volume fractions exhibited different compressive strengths. Therefore, composite materials with appropriate strengths can be selected as thermal insulation materials for the ITP-coring device according to the demands of the coring depths to be used. For every 100 m depth below the ground surface, the rock pressure increases by approximately 2.5 MPa [44].

Taking a coring depth of 2000 m as an example, the rock pressure is approximately 50 MPa. Composite materials with a 60% HGM volume fraction can be selected as the thermal insulation material for the ITP-coring device and ensure the best thermal insulation performance.

3.5. *Density.* Density is one of the main factors affecting a material's thermal insulation performance. Generally, a lower material density leads to a lower proportion of heat-conducting medium, a lower thermal conductivity, and better insulation performance. Since the density of K1 HGMs is much lower than that of the EP matrix, an increase in the HGM volume fraction should lead to a decreased density of the composite material. Figure 11 shows that an increase in the HGM filling amount increased the extent of mutual extrusion, and destruction of the HGMs became more common. However, when a certain number of HGMs was added, the number of damaged HGMs was far less than the number of filled HGMs, so the density decreased regularly with increasing HGM volume fraction.

3.6. *Thermal Insulation Performance.* Within the environment and structure of the ITP-coring device, the performance of the thermal insulation materials mainly depends on their thermal conductivity [45]. The lower the thermal conductivity, the better the insulation performance of the material. The thermal conductivities of the HGMs are lower than that of the EP matrix [46]. Figure 12 shows that the thermal conductivity of the composite decreased gradually with increasing HGM volume fraction. When the HGM volume fraction was increased to 60%, the thermal conductivity of the composite material reached its lowest value, 0.137 W/m·K.

After immersion in water at a pressure of 45 MPa for 2 h, the surface of the material absorbed water, which resulted in a slight increase in thermal conductivity. Figures 9 and 12 show that, overall, absorption of more water by the composite materials under high water pressure led to higher thermal conductivities.

4. Conclusions

Studies of EP properties demonstrated that the mPDA EP was a high-strength matrix for composite insulation materials. Then, composite insulation materials suitable for different coring depths were prepared by combining the EP and HGMs. The applicability of the resulting composite insulation material under high water pressure (45 MPa) was verified in high-pressure water-loading experiments. The conclusions are as follows:

(1) Based on the mechanical strength and thermal stability of the EP, mPDA was selected as the curing agent for the EP matrix from among several curing agents tested

(2) The HGM/EP composite insulation materials exhibited high thermal stability. The thermal decomposition temperatures of composite materials with different HGM volume fractions were above 350°C, which is suitable for the ITP-coring device

(3) The compressive strengths of the HGM/EP composite insulation materials decreased with increasing HGM volume fraction. When the HGM volume fraction was increased by 50%, the compressive strength of the composite materials reached approximately 51.2 MPa and the strength of the composite tended to be stable

(4) The thermal conductivities of the HGM/EP composite insulation materials decreased with increasing HGM volume fraction. When the HGM volume fraction reached its maximum value of 60%, the thermal conductivity reached its minimum value of 0.137 W/m·K

The high-strength thermal insulation materials developed in this paper can be used for deep ITP-coring devices. In addition, due to their low density, high strength, and high insulation performance, they can also be applied to deep-sea buoyancy materials, deep-sea pipeline insulation materials, aerospace insulation materials, etc.

Data Availability

The data that support the findings of this study are available from the corresponding author upon reasonable request.

Conflicts of Interest

The authors declare that there is no conflict of interest regarding the publication of this paper.

Acknowledgments

References

[1] H. P. Xie, F. Gao, Y. Ju et al., "Theoretical and technological conception of the fluidization mining for deep coal resources," *Journal of China Coal Society*, vol. 42, no. 3, pp. 547–556, 2017.

[2] H. P. Xie, F. Gao, Y. Ju et al., "Quantitative definition and investigation of deep mining," *Journal of China Coal Society*, vol. 40, no. 1, pp. 1–10, 2015.

[3] H. P. Xie, H. W. Zhou, D. J. Xue, H. W. Wang, R. Zhang, and F. Gao, "Research and consideration on deep coal mining and critical mining depth," *Journal of China Coal Society*, vol. 37, no. 4, pp. 535–542, 2012.

[4] H. P. Xie, F. Gao, and Y. Ju, "Research and development of rock mechanics in deep ground engineering," *Chinese Journal of Rock Mechanics and Engineering*, vol. 11, no. 34, pp. 2162–2178, 2015.

[5] J. N. Li, J. Wang, Y. Q. Hu et al., "Contact performance analysis of pressure controller's sealing interface in deep in-situ pressure-preserved coring system," *Petroleum Science*, 2021.

[6] M. Z. Gao, J. Xie, J. Guo, Y. Lu, Z. He, and C. Li, "Fractal evolution and connectivity characteristics of mining-induced crack networks in coal masses at different depths," *Geomechanics and Geophysics for Geo-Energy and Geo-Resources*, vol. 7, no. 1, pp. 1–15, 2021.

[7] H. P. Xie, M. Z. Gao, R. Zhang, G. Y. Peng, W. Y. Wang, and A. Q. Li, "Study on the mechanical properties and mechanical response of coal mining at 1000 m or deeper," *Rock Mechanics and Rock Engineering*, vol. 52, no. 5, pp. 1475–1490, 2019.

[8] M. Gao, Z. Zhang, Y. Xiangang, C. Xu, Q. Liu, and H. Chen, "The location optimum and permeability-enhancing effect of a low-level shield rock roadway," *Rock Mechanics and Rock Engineering*, vol. 51, no. 9, pp. 2935–2948, 2018.

[9] G. Mingzhong, H. Haichun, X. Shouning et al., "Discing behavior and mechanism of cores extracted from Songke-2 well at depths below 4,500 m," *International Journal of Rock Mechanics and Mining Sciences*, vol. 149, p. 104976, 2022.

[10] B. G. Yang, M. Z. Gao, J. Xie et al., "Exploration of weakening mechanism of uniaxial compressive strength of deep sandstone under microwave irradiation," *Journal of Central South University*, vol. 29, no. 2, pp. 611–623, 2022.

[11] B. Liang, H. M. Gao, and Y. W. Lan, "Theoretical analysis and experimental study on relation between rock permeability and temperature," *Chinese Journal of Rock Mechanics and Engineering*, vol. 24, no. 12, pp. 2009–2012, 2005.

[12] L. Chen, Y. J. Chu, Y. Zhang, F. Hanand, and J. Zhang, "Analysis of heat transfer characteristics of fractured surrounding rock in deep underground spaces," *Mathematical Problems in Engineering*, vol. 2019, Article ID 1926728, 11 pages, 2019.

[13] M. Z. Gao, J. G. Zhang, S. W. Li, M. Wang, Y. W. Wang, and P. F. Cui, "Calculating changes in fractal dimension of surface cracks to quantify how the dynamic loading rate affects rock failure in deep mining," *Journal of Central South University*, vol. 27, no. 10, pp. 3013–3024, 2020.

[14] J. Xie, M. Z. Gao, R. Zhang, G. Peng, T. Lu, and F. Wang, "Experimental investigation on the anisotropic fractal characteristics of the rock fracture surface and its application on the fluid flow description," *Journal of Petroleum Science and Engineering*, vol. 191, p. 107190, 2020.

[15] H. P. Xie, F. Gao, Y. Ju, R. Zhang, M. Gao, and J. Deng, "Novel idea and disruptive technologies for the exploration and research of deep earth," *Advanced Engineering Sciences*, vol. 1, no. 49, pp. 1–8, 2017.

[16] M. Z. Gao, M. Y. Wang, and J. Xie, "In-situ disturbed mechanical behavior of deep coal rock," *Journal of China Coal Society*, vol. 45, no. 8, pp. 2691–2703, 2020.

[17] M. Z. Gao, B. G. Yang, J. Xie et al., "The mechanism of microwave rock breaking and its potential application to rock-breaking technology in drilling," *Petroleum Science*, 2022.

[18] J. Xie, M. Z. Gao, S. Zhang, C. H. Fu, G. Y. Peng, and J. J. Liu, "Experimental study on triaxial fracture behavior and energy release law of deep coal under the effect of loading rates," *Journal of Central South University (Science and Technology)*, vol. 52, no. 08, pp. 2713–2724, 2021.

[19] M. Z. Gao, J. Xie, Y. N. Gao et al., "Mechanical behavior of coal under different mining rates: a case study from laboratory experiments to field testing," *International Journal of Mining Science and Technology*, vol. 31, no. 5, pp. 825–841, 2021.

[20] H. P. Xie, Y. Ju, M. Gao et al., "Theories and technologies for in-situ fluidized mining of deep underground coal resources," *Journal of China Coal Society*, vol. 43, no. 5, pp. 1210–1219, 2018.

[21] B. S. Nie, J. Gong, X. T. Wang, and C. Peng, "Technological conception of in-situ pulverized coal combustion and explosion power generation based on the deep fluidization mining," *Journal of Mining Science and Technology*, vol. 6, no. 3, pp. 271–279, 2021.

[22] W. Huang, G. Feng, H. L. He, J. Z. Chen, J. Q. Wang, and Z. Zhao, "Development of an ultra-high-pressure rotary combined dynamic seal and experimental study on its sealing performance in deep energy mining conditions," *Petroleum Science*, 2021.

[23] H. P. Xie, T. Liu, M. Z. Gao et al., "Research on *in-situ* condition preserved coring and testing systems," *Petroleum Science*, vol. 18, no. 6, pp. 1840–1859, 2021.

[24] M. Z. Gao, X. Wang, G. Q. Zhang et al., "The novel idea and technical progress of lunar in-situ condition preserved coring," *Geomechanics and Geophysics for Geo-Energy and Geo-Resources*, vol. 8, no. 2, pp. 1–20, 2022.

[25] Z. Q. He, Y. Yang, B. Yu et al., "Research on properties of hollow glass microspheres/epoxy resin composites applied in deep rock *in-situ* temperature-preserved coring," *Petroleum Science*, 2021.

[26] Y. Q. Hu, J. Xie, S. N. Xue et al., "Research and application of thermal insulation effect of natural gas hydrate freezing corer based on the wireline-coring principle," *Petroleum Science*, 2021.

[27] Y. H. Sun, Y. Wang, X. S. Lü, R. Jia, and W. Guo, "Hole-bottom freezing method for gas hydrate sampling," *Journal of Natural Gas Science and Engineering*, vol. 25, no. 1, pp. 271–283, 2015.

[28] M. Kawasaki, S. Umezu, and M. Yasuda, "Pressure temperature core sampler (PTCS)," *Journal of The Japanese Association for Petroleum Technology*, vol. 71, no. 1, pp. 139–147, 2006.

[29] A. V. Milkov, G. R. Dickens, G. E. Claypool et al., "Co-existence of gas hydrate, free gas, and brine within the regional gas hydrate stability zone at Hydrate Ridge (Oregon margin): evidence from prolonged degassing of a pressurized core," *Earth and Planetary Science Letters*, vol. 222, no. 3-4, pp. 829–843, 2004.

[30] G. Bohrmann, W. F. Kuhs, S. A. Klapp et al., "Appearance and preservation of natural gas hydrate from Hydrate Ridge sampled during ODP Leg 204 drilling," *Marine Geology*, vol. 244, no. 1-4, pp. 1–14, 2007.

[31] Y. D. Zhang, Z. L. Jiang, P. Yu et al., "NGH deepwater shallow hole heat preservation and pressure holding core drilling tool, M," The First Institute of Oceanography, China, 2006.

[32] H. Y. Zhu, Q. Y. Liu, G. R. Wong et al., "A pressure and temperature preservation system for gas-hydrate-bearing sediments sampler," *Petroleum Science and Technology*, vol. 31, no. 6, pp. 652–662, 2013.

[33] H. Y. Zhu, Q. Y. Liu, J. G. Deng et al., "Pressure and temperature preservation techniques for gas-hydrate-bearing sediments sampling," *Energy*, vol. 36, no. 7, pp. 4542–4551, 2011.

[34] J. P. Yang, L. Chen, X. B. Gu et al., "Hollow glass microspheres/silicone rubber composite materials toward materials for high performance deep in-situ temperature-preserved coring," *Petroleum Science*, vol. 19, no. 1, pp. 309–320, 2022.

[35] W. T. Wang and L. Watkins, "Flexible epoxy syntactic foam thermal insulation for high temperature deepsea reelable pipelay installations," in *29th ASME international conference on ocean, Offshore and Arctic Engineering*, pp. 269–273, Shanghai, PEOPLES R CHINA, 2010.

[36] J. Hu, M. Chen, X. S. Fang, and L. M. Wu, "Fabrication and application of inorganic hollow spheres," *Chemical Society Reviews*, vol. 40, no. 11, pp. 5472–5491, 2011.

[37] X. F. Wu, Y. Gao, Y. Wang et al., "Recent developments on epoxy-based syntactic foams for deep sea exploration," *Journal of Materials Science*, vol. 56, no. 3, pp. 2037–2076, 2021.

[38] X. W. Zhao, C. G. Zang, Y. L. Sun, Y. L. Zhang, Y. Q. Wen, and Q. J. Jiao, "Effect of hybrid hollow microspheres on thermal insulation performance and mechanical properties of silicone rubber composites," *Journal of Applied Polymer Science*, vol. 135, no. 11, p. 46025, 2018.

[39] J. Brown, J. Oldenkamp, R. Gamache, D. Grbovic, and E. Kartalov, "Hollow-microsphere composite offers depth-independent superior thermal insulation for diver suits," *Materials Research Express*, vol. 6, no. 5, p. 055314, 2019.

[40] H. Zhou, S. M. Zhang, and M. S. Yang, "The effect of heat-transfer passages on the effective thermal conductivity of high filler loading composite materials," *Composites Science and Technology*, vol. 67, no. 6, pp. 1035–1040, 2007.

[41] J. W. Wang, Y. P. Tian, and J. Zhang, "Thermal insulating epoxy composite coatings containing sepiolite/hollow glass microspheres as binary fillers: morphology, simulation and application," *Science and Engineering of Composite Materials*, vol. 24, no. 3, pp. 379–386, 2017.

[42] N. Gupta, S. Priya, R. Islam, and W. Ricci, "Characterization of mechanical and electrical properties of epoxy-glass microballoon syntactic composites," *Ferroelectrics*, vol. 345, no. 1, pp. 1–12, 2006.

[43] C. B. Sun, Q. H. Wamg, Y. Xing, Z. W. Du, and Q. F. Wang, "High intensity deep sea buoyancy material made from polymer filled with hollow micro-glass ball," *Journal of the Harbin Institute of Technology*, vol. 38, no. 11, pp. 2000–2002, 2006.

[44] H. P. Xie, M. Z. Gao, R. Zhang et al., "Study on concept and progress of in-situ fidelity coring of deep rocks," *Chinese Journal of Rock Mechanics and Engineering*, vol. 39, no. 5, pp. 865–876, 2020.

[45] F. Hu, S. Y. Wu, and Y. G. Sun, "Hollow-structured materials for thermal insulation," *Advanced Materials*, vol. 31, no. 38, p. 1801001, 2019.

[46] Y. J. Qiao, X. D. Wang, X. H. Zhang, and Z. P. Xing, "Thermal conductivity and compressive properties of hollow glass microsphere filled epoxy-matrix composites," *Journal of Reinforced Plastics and Composites*, vol. 34, no. 17, pp. 1413–1421, 2015.